Supporting Information for

Reconciling Electrolyte Donicity and Polarity for Lithium Carbon Fluoride Batteries

Xingxing Wang,[a] Ziyu Song,[a] Hao Wu,[a] Jiayi Chen,[a] Wenfang Feng,[a] Michel Armand,[b] Zhibin Zhou,[a] * and Heng Zhang[a] *

a *Key Laboratory of Material Chemistry for Energy Conversion and Storage (Ministry of Education)*
School of Chemistry and Chemical Engineering, Huazhong University of Science and Technology
1037 Luoyu Road, Wuhan 430074, China

b *Centre for Cooperative Research on Alternative Energies (CIC energigune), Basque Research and Technology Alliance (BRTA)*
Alava Technology Park, Albert Einstein 48, 01510 Vitoria-Gasteiz, Spain

Corresponding Authors

*Z. Zhou: E-mail: zb-zhou@mail.hust.edu.cn.

*H. Zhang: E-mail: hengzhang2020@hust.edu.cn.

Experimental Section

Materials: Lithium bis(trifluoromethanesulfonyl)imide (LiTFSI) salt was obtained from Rhodia (purity > 99.8%). The electrolyte solvents including propylene carbonate (PC), 1,2-dimethoxyethane (DME) were received from Aladdin, and were purified using standard procedures before use. [1] The Whatman GF/A separator (18 mm in diameter, 260 μm in thickness), carbon fluoride powders ($CF_{0.85}$, battery grade, Zhong Ke Ceffone) were dried under vacuum (60 °C, 12 h, < 1 mmHg) before use. The conductive carbon (Super P, battery grade) and aluminum foil (16 μm in thickness) were purchased from Shenzhen Kejing, and the polymeric binder PVdF was received from Arkema. The battery-grade metallic lithium disks (14 mm in diameter, 500 μm in thickness) were obtained from China Energy Lithium Co., Ltd. Sodium bis(trifluoromethylsulfonyl)imide (NaTFSI) was synthesized following previous report. [2-4]

Preparation of the as-resulting electrolytes: The nonaqueous electrolytes comprising various fractions of DME and PC were prepared in an argon-filled glove box (H_2O < 1 ppm, O_2 < 1 ppm), following our previous work. [5] The water content of each electrolyte sample was strictly limited to be lower than 30 ppm (Karl-Fischer titration, Metrohm KF 831).

Preparation of the carbon fluoride cathode: The carbon fluoride cathode sheet comprising $CF_{0.85}$ as active material (85 wt%), super P as conductive carbon (10 wt%), and PVdF as binder (5 wt%) was prepared following previous work. [5] The cathode sheets with an active material loading of 2.0−2.5 mg cm^{-2} were punched into disks (14 mm in diameter) and were vacuum-dried (100 °C, 12 h) before cell assembly.

Characterizations of solvents and electrolytes: The dielectric constant values of the solvent were tested with an electrochemical workstation (Multi Autolab M204, Metrohm) using a cylindrical capacitor cell. [6, 7] The cylindrical capacitor cell was wired in parallel with the variable resistor, and placed in a temperature-controlled box. The impedance was measured from 10^6 to 10^{-1} Hz (amplitude voltage: 10 mV). The value of capacitance was obtained by fitting the EIS spectra with a RC multiple circuit. The measured capacitance of the reference solvents is closely associated to the dielectric constant, giving a linear regression equation (R^2 = 0.9986) shown in Figure S2.

The Gutmann donor number (DN) of the solvents was determined with the help of ^{23}Na NMR spectroscopy (Bruker Avance 400, Switzerland), using 0.01 M solution of NaTFSI in different DME/PC solvents. The DN values of various solvents are calculated by Equation (S1), [8]

$$DN = 2.106 \times \delta + 32.74 \qquad \text{Equation (S1)}$$

where δ is the chemical shift of ^{23}Na in NMR spectra.

The polarity of solvents in $E_T(30)$ scale was determined by UV–vis absorption spectroscopy. Appropriate aliquots of the indicator and solvents were prepared, and the as-formed steady–state solution was transferred into the quartz cuvette (final probe concentrations were ca. 1×10^{-4} mol L^{-1}). UV–vis absorption spectra of the solutions were recorded by using a UV–vis spectrophotometer (UV 2600, Shimadzu).

The measurement of ionic conductivities (σ) was carried out using an Multi Autolab M204 impedance analyzer. The conductivity cells with two platinized platinum disks (cell constant: ca. 10 cm^{-1}) were prepared in an argon-filled glove box. The testing temperature of the cell was accurately controlled by a JULABO RTH oil bath (± 0.1 °C). Raman spectra of the electrolyte and solvent samples were recorded with a Renishaw in confocal Raman spectrometer (LabRAM HR800; wavelength of incident laser: 532 nm). The samples were hermetically sealed in a nuclear magnetic tube and the spectra were collected in the range spanning from 200 to 2200 cm^{-1}.

Cell testing: The galvanostatic discharge tests of 2032-type coin cells were achieved on a Neware battery testing apparatus in a temperature-controlled room (25±1 °C). These as-resulting samples discharged over different current-rates (i.e., 0.05C, 0.1C, 0.5C, 1C, and 2C) with a cut-off voltage at 1.5 V. Before discharge, the cells were left under open circuit voltage (OCV) for 10 h, aiming to avoid interference from the external condition. The galvanostatic intermittent titration technique (GITT) measurement of 2032-type coin cells were performed on a LAND battery cycler (CT2001) at 25 °C. The measurement procedure was set to a pulse current of 0.1C for 30 mins followed by a rest interval for 2.5 h and a cut-off voltage at 1.5 V.

The corresponding D_{Li}^+ could be calculated through the following Equation (S2) by applying the Fick's second law: [9-11]

$$D_{Li}^{+} = \frac{4}{\pi}\left(\frac{I_0 V_M}{Z_i F S}\right)\left(\frac{dE/dx}{dE/d\sqrt{\tau}}\right)^2 \quad \left(\tau \ll L^2/D_{Li}^{+}\right) \qquad \text{Equation (S2)}$$

Where I_0, Z_i and V_M is the set current and the charge transfer number in the discharge process, and the molar volume of the CF_x cathode material, respectively; F, S and L is the Faraday constant, the total contact area between the electrode and the electrolyte, and the thickness of the electrode, respectively, dE/dx is the slope of the coulometric titration curve, dE/d$\sqrt{t}$ is the transient voltage change during the single titration current flux (after subtracting the IR drop).

Bulk and surface characterizations of CF_x cathode: The X-ray diffraction (XRD) patterns of the electrodes were recorded on an X-ray diffractometer (Smart Lab-SE, Rigaku Corporation) with Cu-Kα (λ = 1.54056 Å, incident wavelength) radiation. The XRD patterns were measured in the incident X-ray angles (2ϑ) ranging from 5 to 80° at a scan rate of 10° min^{-1}. A field emission scanning electron microscope (FE-SEM, SU8010, Hitachi) technology was performed to observe the morphological micro-structures of the fresh and fully discharged carbon fluoride materials. The elemental composition of fresh $CF_{0.85}$ cathodes and cathodes after discharge were analyzed by the EDX and XPS measurements using a photoelectron spectrometer (AXIS-ULTRA DLD-600W, Shimadzu) and the Al Kα source.

Table S1 Summarization of solvent parameters such as permittivity, polarity, and donicity with the various fraction of PC content at 25 °C.

Samples	Abbreviations	Permittivity	Polarity / kcal mol^{-1}	Donicity / kcal mol^{-1}
DME	$D_{100}P_0$	7.5	37.9	20.6
PC/DME (30:70, by wt)	$D_{70}P_{30}$	18.2	42.7	18.7
PC/DME (50:50, by wt)	$D_{50}P_{50}$	31.4	44.0	17.7
PC/DME (70:30, by wt)	$D_{30}P_{70}$	41.4	44.7	17.1
PC	D_0P_{100}	64.0	46.0	13.4

Table S2 Corresponding Cartesian coordinates of the optimized structures for the PC and DMC solvent using DFT calculations.

Atom	*x*	*y*	*z*	Atom	*x*	*y*	*z*
PC				DMC			
O	−3.50063	−0.00133	−0.07594	C	−3.07712	1.25858	−0.00998
C	−2.30651	0.63039	−0.21664	O	−1.80019	1.91161	−0.0526
O	−1.28976	−0.24412	−0.02201	H	−3.18657	0.57759	−0.85085
C	−3.28451	−1.41006	0.06317	H	−3.81005	2.05579	−0.06806
C	−1.8041	−1.50972	0.44447	H	−3.19073	0.70327	0.9184
H	−3.49691	−1.89517	−0.89101	C	−0.74188	1.09858	−5.7285E-4
H	−3.95651	−1.79368	0.82564	O	0.36053	1.85143	−0.04036
C	−1.04359	−2.65402	−0.18318	C	1.59882	1.12774	0.00141
H	−1.68587	−1.52112	1.52994	H	1.66304	0.53171	0.90876
H	−1.44003	−3.60422	0.17656	H	2.37511	1.88487	−0.01271
H	0.01045	−2.60482	0.08216	H	1.68812	0.47462	−0.86384
H	−1.13197	−2.62804	−1.26842	O	−0.77578	−0.10249	0.07049
O	−2.17627	1.78122	−0.47374				

The Fritz Haber Institute ab initio molecular simulations (FHI-aims) software was used as a platform for performing the DFT calculations.[12, 13] The Becke's three parameters (B3) exchange functional in combination with the Lee–Yang–Parr (LYP) nonlocal correlation functional (B3LYP)[14] was implemented.[15] For generating initial geometries of the PC and DMC solvent, the open-source molecular visualizer Avogadro was used.[16] Detailed procedures could be accessed in our previous work.[17-19]

Table S3 Some selected polarity scales defined by the kinetic and spectroscopic measurement, respectively.

Entry	Polarity scale	Definition	Comments	Ref.
1	Y	$\mathrm{Y} = \log\frac{k}{k_o}/m$ k — The rate constant for *t*-butyl chloride in the given solvent (s^{-1}); k_o — The rate constant for t-butyl chloride in the standard solvent (s^{-1}); m — A slope characteristic of each substance;	The ionizing power of t-butyl chloride in the given solvent	20-22
2	Ω	$\Omega = \log\frac{k_N}{k_X} = \log\frac{N}{X}$ k_N — The rate constants for forming endo-product (s^{-1}); k_X — The rate constants for forming exo-product (s^{-1});	The product of the specific rate constants for forming endo-product (k_N), against that for forming exo-product (k_X)	23
3	Z	$Z = E_T = 2.859\cdot10^{-3}\cdot\nu$ E_T — The molar transition energies (kcal·mol^{-1}); ν — The position of the absorption maximum (cm^{-1});	The molar transition energies of 1-ethyl-4-methoxycarbonylpyridinium iodide	24
4	$E_T(30)$	$E_T(30) = 28591/\lambda_{max}$ λ_{max} — The maximum wavelength of the absorption band in the ultraviolet-visible (UV-vis) region (nm);	The molar electronic transition energy (historically in kcal·mol^{-1}) of the Reichardt dye 30	25, 26

Table S4 Molar absorption coefficient of these involved solvent samples, calculated by the Beer-Lamber law.

Sample	A [a)]	b [b)] / cm	c [c)] / mol L^{-1}	k [d)] / L cm^{-1} mol^{-1}
DME-dye 30	0.625	1	1×10^{-4}	6.25×10^{3}
DME/PC (7:3, w/w)-dye 30	0.654	1	1×10^{-4}	6.54×10^{3}
DME/PC (5:5, w/w)-dye 30	0.411	1	1×10^{-4}	4.11×10^{3}
DME/PC (3:7, w/w)-dye 30	0.372	1	1×10^{-4}	3.72×10^{3}
PC-dye 30	0.481	1	1×10^{-4}	4.81×10^{3}

a) Absorbance of the sample; b) Thickness of cuvette; c) Solution concentration; d) Molar absorption coefficient of the sample.

Table S5 Summarization of the specific capacity, voltage plateau and energy density of all the samples on the discharged CF_x cathode by XPS technology at 0.1C.

Samples	Abbreviations	Specific capacity / mAh g^{-1}	Voltage plateau / V	Energy density / Wh kg^{-1}
LiTFSI-DME	$D_{100}P_0$	649.2	2.92	1754.4
LiTFSI-PC/DME (30:70, by wt)	$D_{70}P_{30}$	678.2	2.93	1843.7
LiTFSI-PC/DME (50:50, by wt)	$D_{50}P_{50}$	636.2	2.86	1700.6
LiTFSI-PC/DME (70:30, by wt)	$D_{30}P_{70}$	578.1	2.83	1531.4
LiTFSI-PC	D_0P_{100}	202.3	2.58	494.3

Table S6 Atomic percentage for the elements detected on the discharged CF_x cathode by EDX technology.

Samples	C / at.%	N / at.%	O / at.%	F / at.%	S / at.%
Fresh $CF_{0.85}$	72.94			27.06	
$D_{100}P_0$	57.36	1.72	4.53	36.01	0.39
$D_{70}P_{30}$	53.95	0.00	8.32	36.96	0.76
$D_{50}P_{50}$	57.66	2.04	7.80	32.23	0.26
$D_{30}P_{70}$	58.68	0.00	2.89	38.24	0.19
D_0P_{100}	65.83	0.00	2.57	31.42	0.18

Table S7 Atomic percentage for the elements detected on the discharged CF_x cathode by XPS technology.

Samples	C / at.%	O/ at.%	F / at.%	Li / at.%	S / at.%	N / at.%
$D_{100}P_0$	21.8	26.3	31.7	18.4	1.1	0.8
$D_{70}P_{30}$	41.7	24.4	14.1	18.6	0.5	0.6
$D_{50}P_{50}$	32.9	22.1	28.8	15.5	0.1	0.6
$D_{30}P_{70}$	27.6	30.1	28.1	13.5	0.2	0.6
D_0P_{100}	30.2	25.5	26.2	14.5	3.2	0.7

Table S8 Summarization of the deconvoluted peak positions and area in the region of 675–775 and 775–900 cm^{-1} in the Raman spectroscopy for the various electrolytes at 25 °C.

Samples	Peak position / cm^{-1}	Peak area	Ref.
$D_{100}P_0$	739 (Free $TFSI^-$)	30264	27, 28
	821 (Free DME)	12928	
	847 (Free DME)	25319	
	872 (Solvated Li^+-DME)	17558	
$D_{70}P_{30}$	709 (Free PC)	11201	29-38
	727 (Solvated Li^+-PC)	1554	
	739 (Free $TFSI^-$)	24558	
	823 (Free DME)	6299	
	847 (Free DME and PC)	34696	
	872 (Solvated Li^+-DME)	12383	
$D_{50}P_{50}$	709 (Free PC)	20308	29-38
	727 (Solvated Li^+-PC)	2389	
	739 (Free $TFSI^-$)	27402	
	825 (Free DME)	5047	
	847 (Free DME and PC)	47701	
	872 (Solvated Li^+-DME)	12517	
$D_{30}P_{70}$	709 (Free PC)	26124	29-38
	726 (Solvated Li^+-PC)	2407	
	739 (Free $TFSI^-$)	25628	
	826 (Free DME)	2168	
	847 (Free DME and PC)	52421	
	872 (Solvated Li^+-DME)	7830	
D_0P_{100}	709 (Free PC)	33111	29, 30, 32, 36, 37, 39
	726 (Solvated Li^+-PC)	4554	
	739 (Free $TFSI^-$)	21438	
	847 (Free PC)	59572	

Table S9 Summary of various parameters and reaction mechanism for conversion-type electrode materials.

Classification	Materials	Theoretical capacity / mAh g^{-1}	Work potential / V	Reaction mechanism	Ref.
Oxides	CuO	670	0 – 3	$CuO + 2Li \leftrightarrow Cu + Li_2O$	40, 41
	NiO	718	0.005 – 3	$NiO + 2Li \leftrightarrow Ni + Li_2O$	41
	Fe_2O_3	1005	0.01 – 3	$Fe_2O_3 + 6Li \leftrightarrow 2Fe + 3Li_2O$	42
	Fe_3O_4	926	0 – 3	$Fe_3O_4 + 8Li \leftrightarrow 3Fe + 4Li_2O$	43
	MnO_2,	1230	0.35	$MnO_2 + 4Li \leftrightarrow Mn + 2Li_2O$	44
	$MnFe_2O_4$,	765	0.8	$MnFe_2O_4 + 8Li \leftrightarrow Mn + 2Fe + 4Li_2O$	45
	SnO_2,	1493	1.0	$SnO_2 + 4Li \leftrightarrow Sn + 2Li_2O$	46
	ZnO	988	0.7	$ZnO + 2Li \leftrightarrow Zn + Li_2O$	47
Chalcogenides	S	1675	2.2	$S_8 + 16Li \leftrightarrow 8Li_2S$	48
	CoS_2	870		$CoS_2 + 4Li \leftrightarrow Co + 2Li_2S$	49
	FeS_2	894	1.87	$FeS_2 + 4Li \leftrightarrow Fe + 2Li_2S$	50
	Cu_2S	335	0.5	$Cu_2S + 2Li \leftrightarrow 2Cu + Li_2S$	51
	TiS_2	239		$TiS_2 + 4Li \leftrightarrow Ti + 2Li_2S$	52
	SnS_2	1231		$SnS_2 + 4Li \leftrightarrow Sn + 2Li_2S$	53, 54
	Sb_2Se_3	670	0.86	$Sb_2Se_3 + 12Na \leftrightarrow 2Na_3Sb + 3Na_2Se$	55
Fluorides	FeF_3	712	2.7	$FeF_3 + 3Li \leftrightarrow Fe + 3LiF$	56
	NiF_2	320	1.3	$NiF_2 + 3Li \leftrightarrow Ni + 2LiF$	57
	$Cu_yFe_{1-y}F_2$	549	2.8, 3.4, 3.8	$Cu_yFe_{1-y}F_2 + 2Li \leftrightarrow yCu + 1-yFe + 2LiF$	58
Phosphides	Ni_2P	2596		$Ni_2P + 3Na \leftrightarrow 2Ni + Na_3P$	59, 60
Silicates	Co_2SiO_4		1.6		61

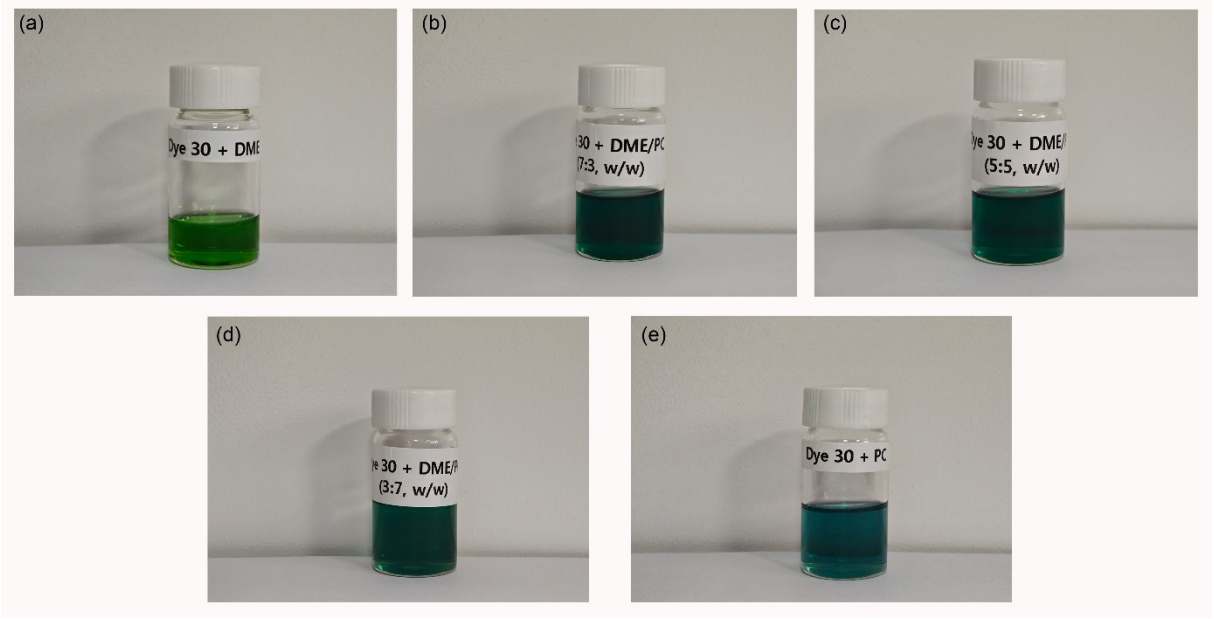

Fig. S1. Appearance photos of different solvent after adding dye 30: (a) dye 30 + DME, (b) dye 30 + DME/PC (7:3, by wt.), (c) dye 30 + DME/PC (5:5, by wt.), (d) dye 30 + DME/PC (3:7, by wt.), (e) dye 30 + PC.

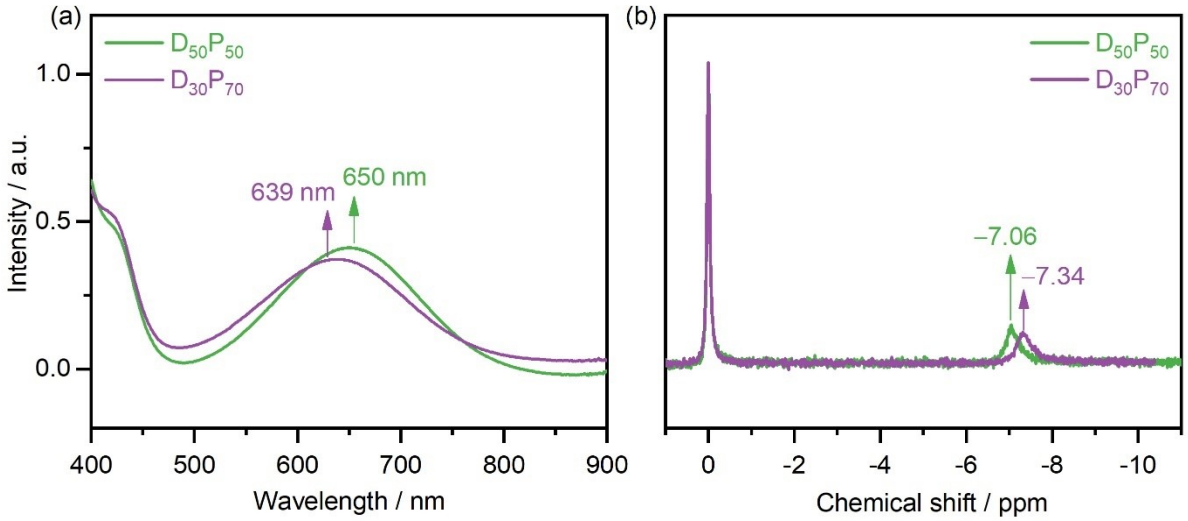

Fig. S2 (a) UV-vis absorption spectra of the different DME/PC mixed electrolytes (i.e., $D_{50}P_{50}$ and $D_{30}P_{70}$) in the range of 400–900 nm. (b) ^{23}Na-NMR spectra of the different DME/PC mixed electrolytes (i.e., $D_{50}P_{50}$ and $D_{30}P_{70}$) with NaTFSI.

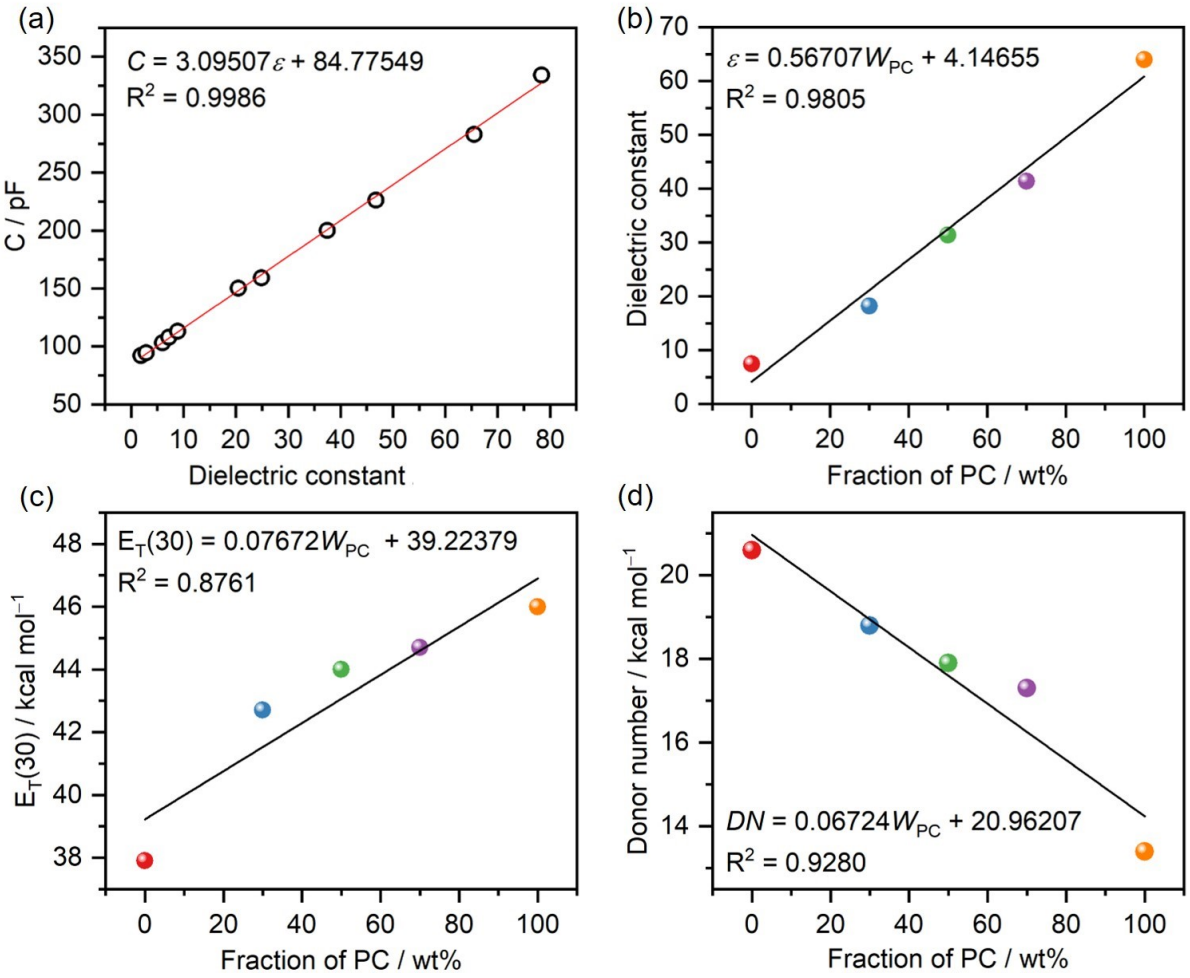

Fig. S3 (a) Dielectric constant of the DME/PC mixed solvents measured by the method suggested by Dahn et al.[7] The dielectric constants of the used reference solvents are given below: 1.9 (*n*-hexane), 2.9 (ethyl methyl carbonate), 6.0 (ethyl acetate), 7.2 (1,2-dimethoxyethane), 8.9 (dichloromethane), 20.5 (acetone), 24.9 (ethanol), 37.5 (acetonitrile), 46.8 (dimethyl sulfoxide), 65.5 (propylene carbonate), and 78.4 (water).[62-64] The fitting curves and equations of the solvent parameters for five kinds of PC/DME mixtures: (b) dielectric constant; (c) $E_T(30)$ value; (d) Donor number value.

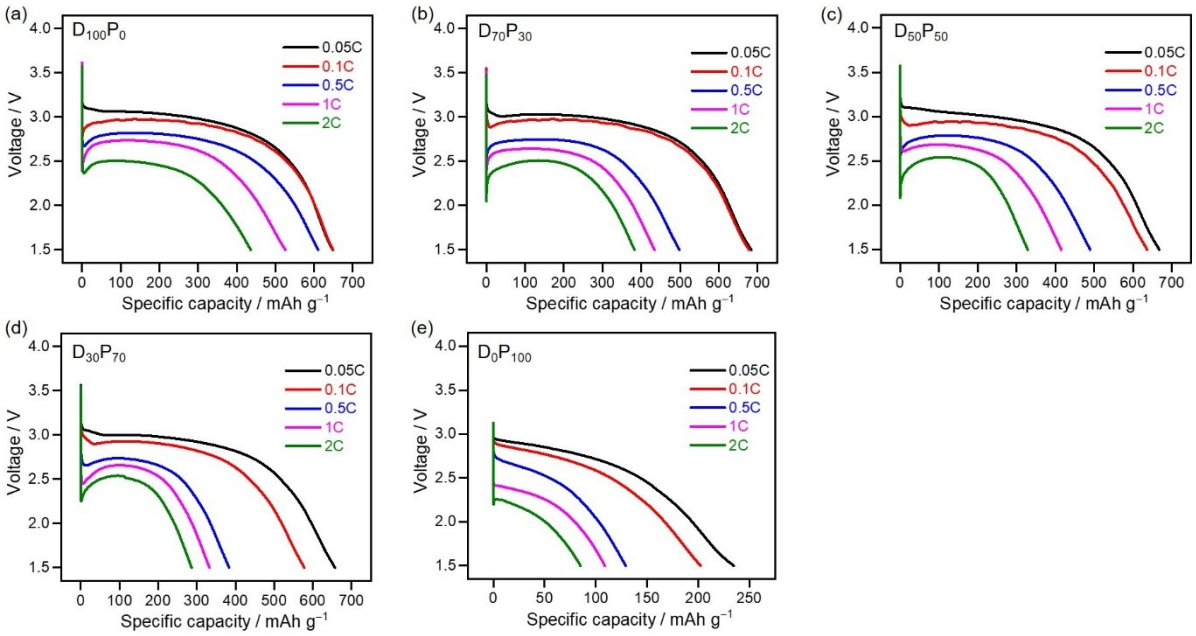

Fig. S4. Dependence of discharged capacities vs. current-rates for the Li°||CF_x cells with different electrolytes, (a) $D_{100}P_0$, (b) $D_{70}P_{30}$, (c) $D_{50}P_{50}$, (d) $D_{30}P_{70}$, and (e) D_0P_{100}.

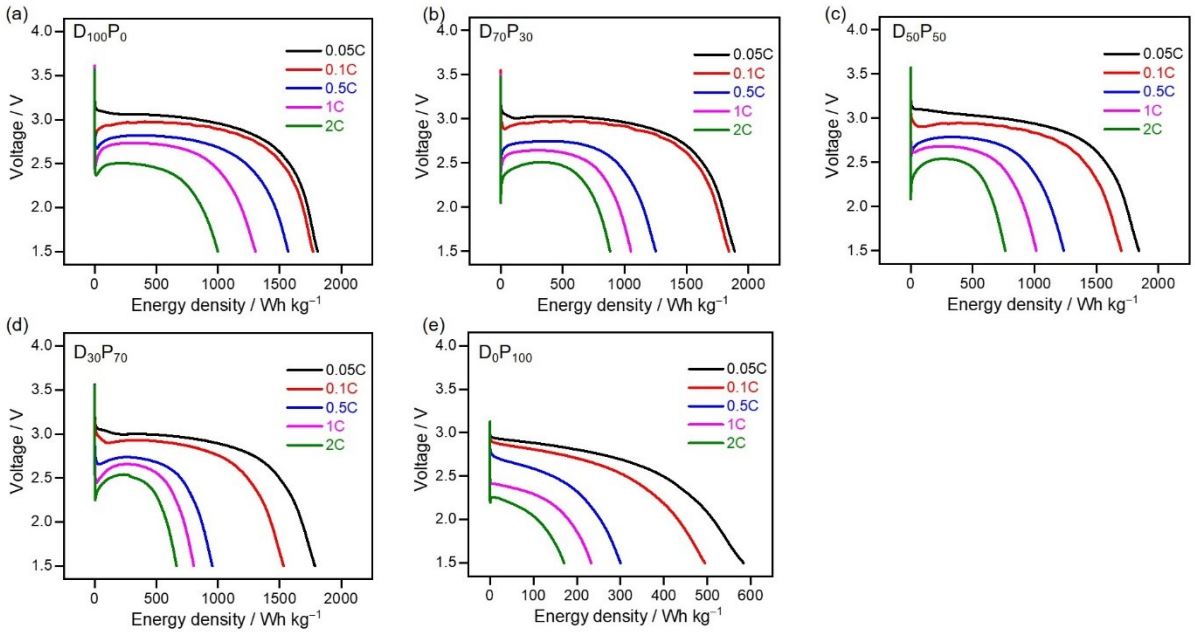

Fig. S5 Dependence of energy density vs. current-rates for the Li°||CF_x cells with different electrolytes, (a) $D_{100}P_0$, (b) $D_{70}P_{30}$, (c) $D_{50}P_{50}$, (d) $D_{30}P_{70}$, and (e) D_0P_{100}.

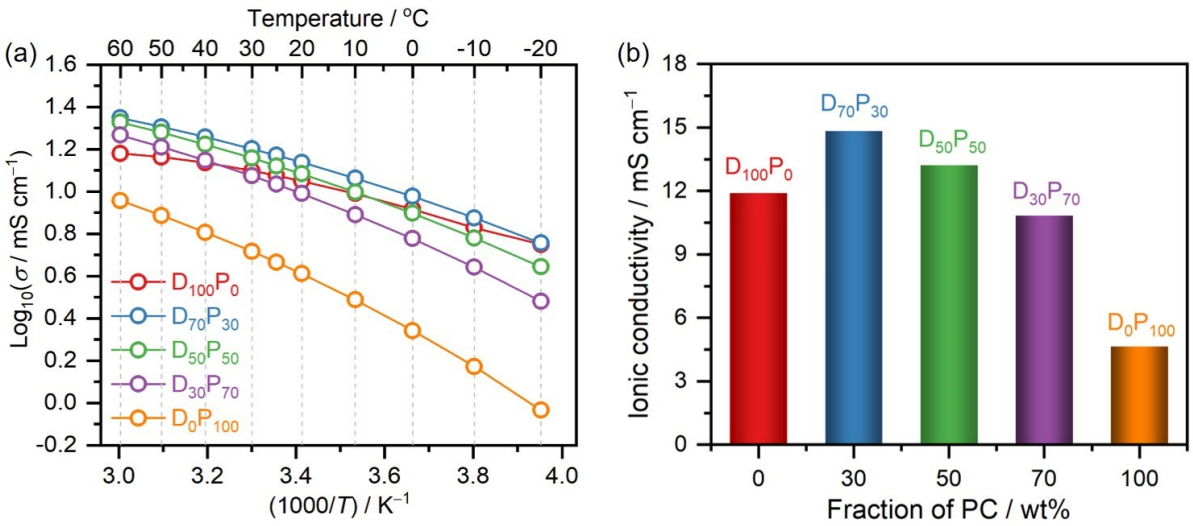

Fig. S6 (a) Temperature dependence of ionic conductivities for various kinds of electrolytes. (b) Ionic conductivities of the electrolytes at 25 °C.

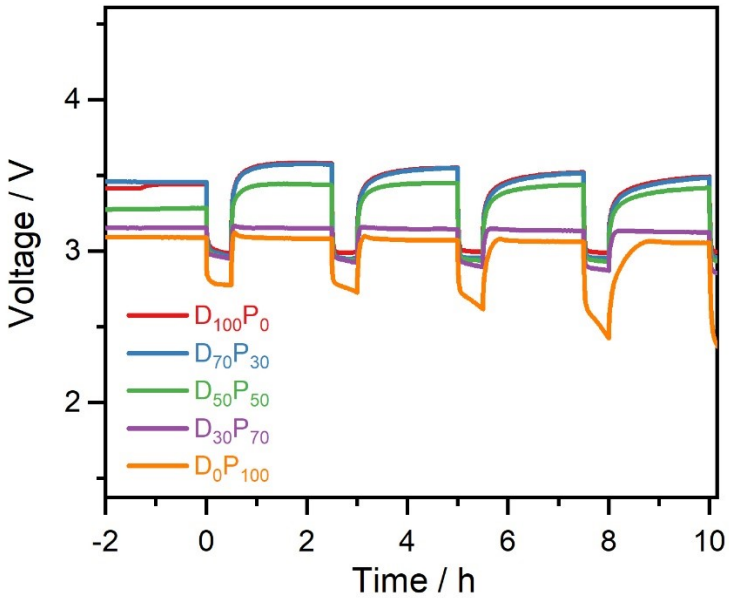

Fig. S7 Zoomed-in profiles of the Li°||CF_x cells with different electrolytes at a relatively low discharge rate of 0.1C.

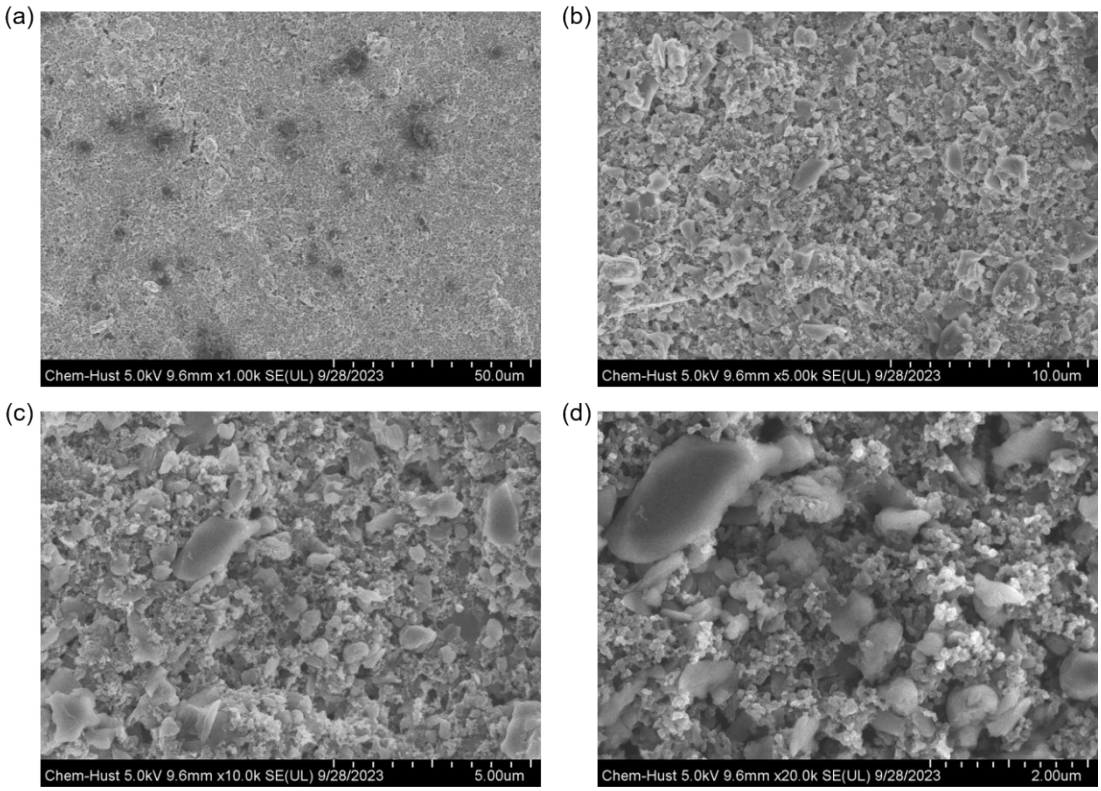

Fig. S8 SEM images of the fresh CF_x cathode at various magnification scale. (a) × 1000, (b) × 5000, (c) × 10000, (d) × 20000.

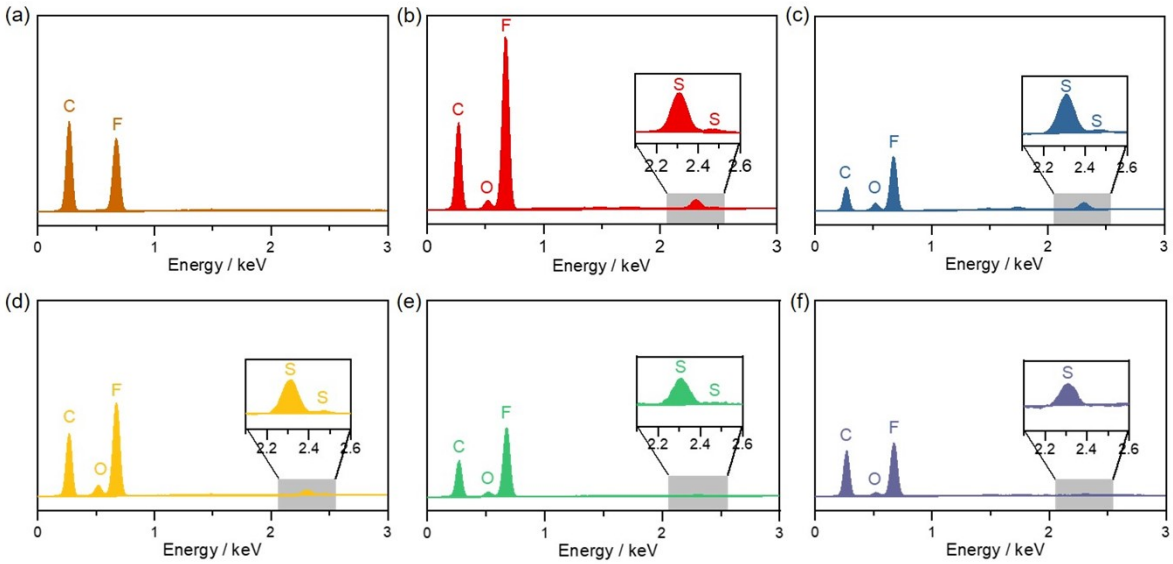

Fig. S9 Energy-dispersive X-ray spectra of pristine fluorinated carbon (a) and the electrodes after discharge at 0.1C with various kinds of electrolytes (b-f). (b) $D_{100}P_0$, (c) $D_{70}P_{30}$, (d) $D_{50}P_{50}$, (e) $D_{30}P_{70}$, and (f) D_0P_{100}.

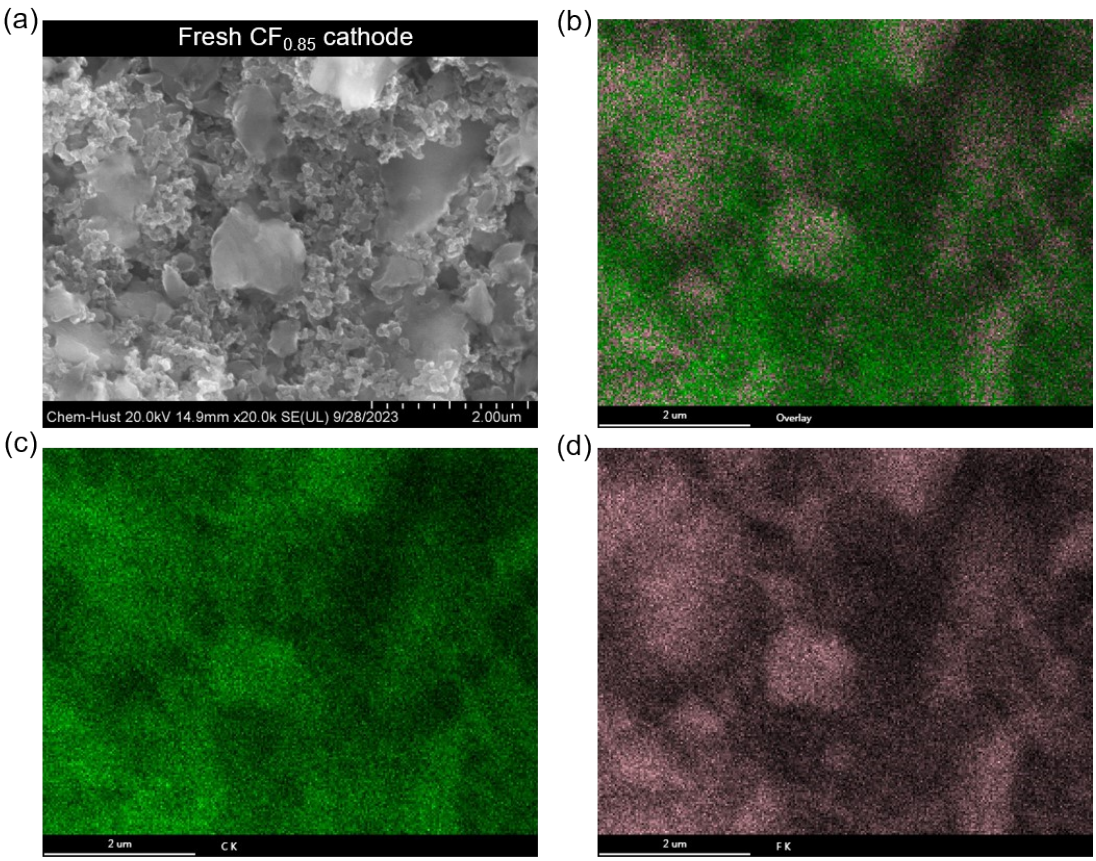

Fig. S10 EDX images of the fresh CF_x cathodes: (a) region selected for mapping analyses, (b) overlay of element C and F signals, (c) element C signal, and (d) element F signal.

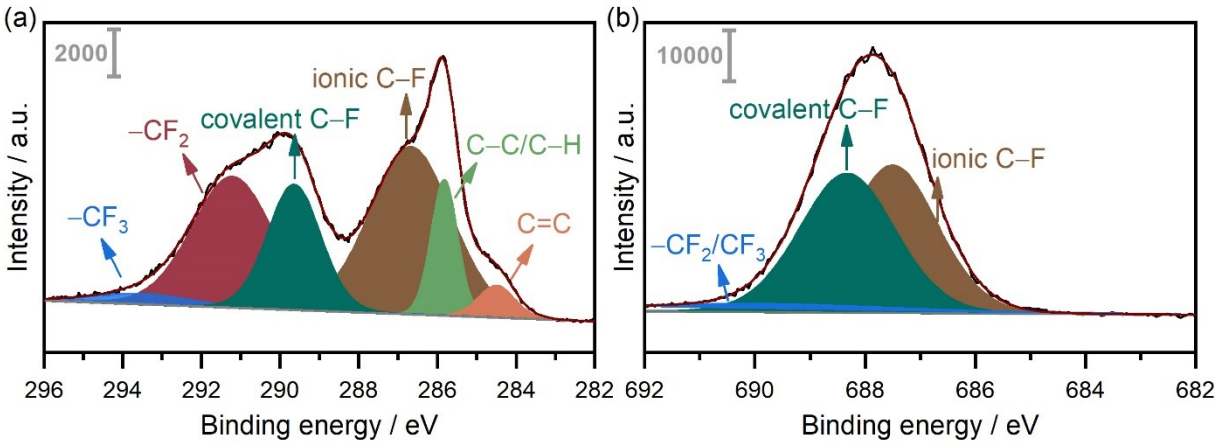

Fig. S11 (a) C 1s and (b) F 1s XPS spectra of the fresh CF_x cathode.

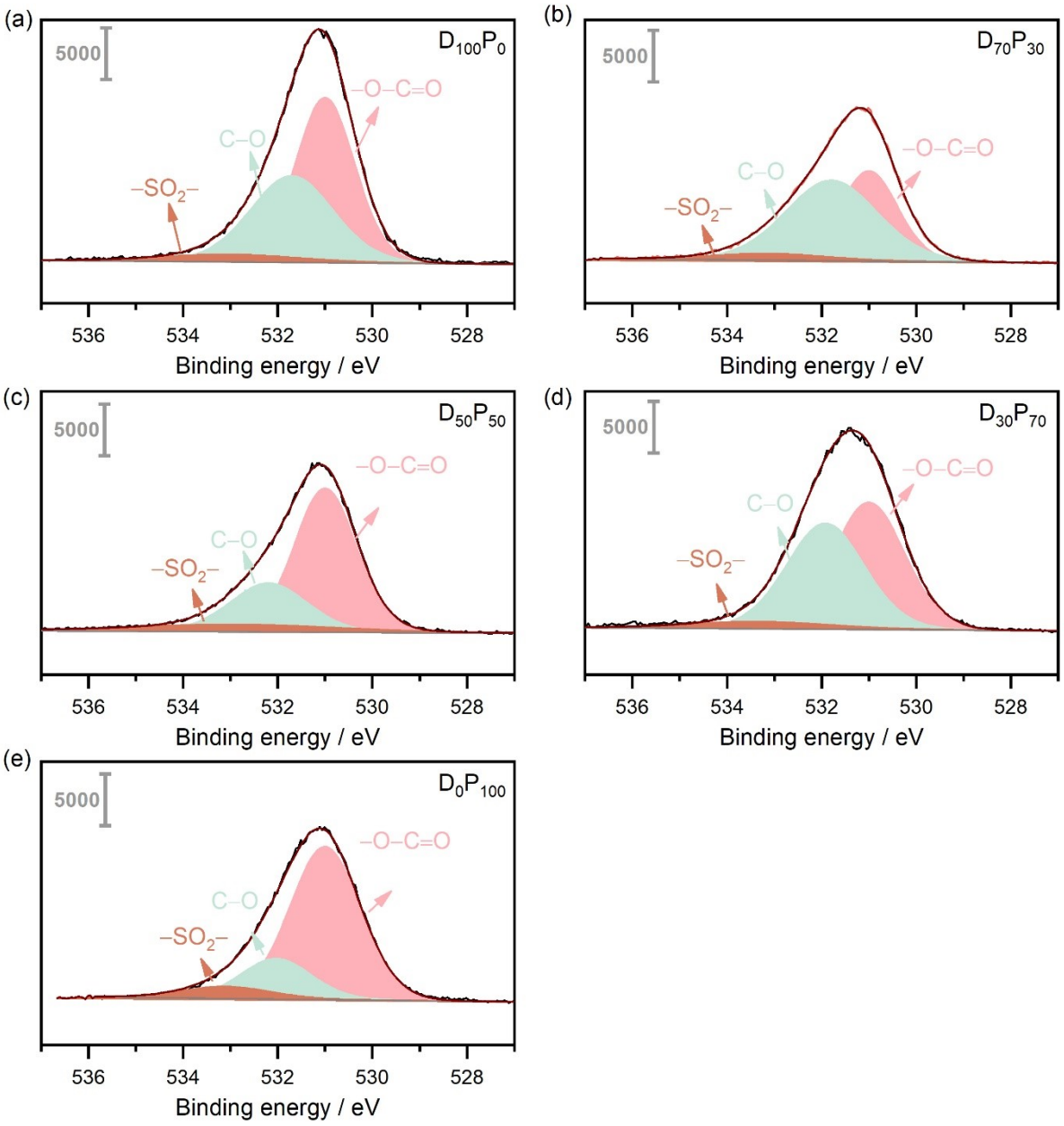

Fig. S12 O 1s XPS spectra for the CF_x cathodes after discharge at 0.1C in various kinds of electrolytes: (a) $D_{100}P_0$, (b) $D_{70}P_{30}$, (c) $D_{50}P_{50}$, (d) $D_{30}P_{70}$, and (e) D_0P_{100}.

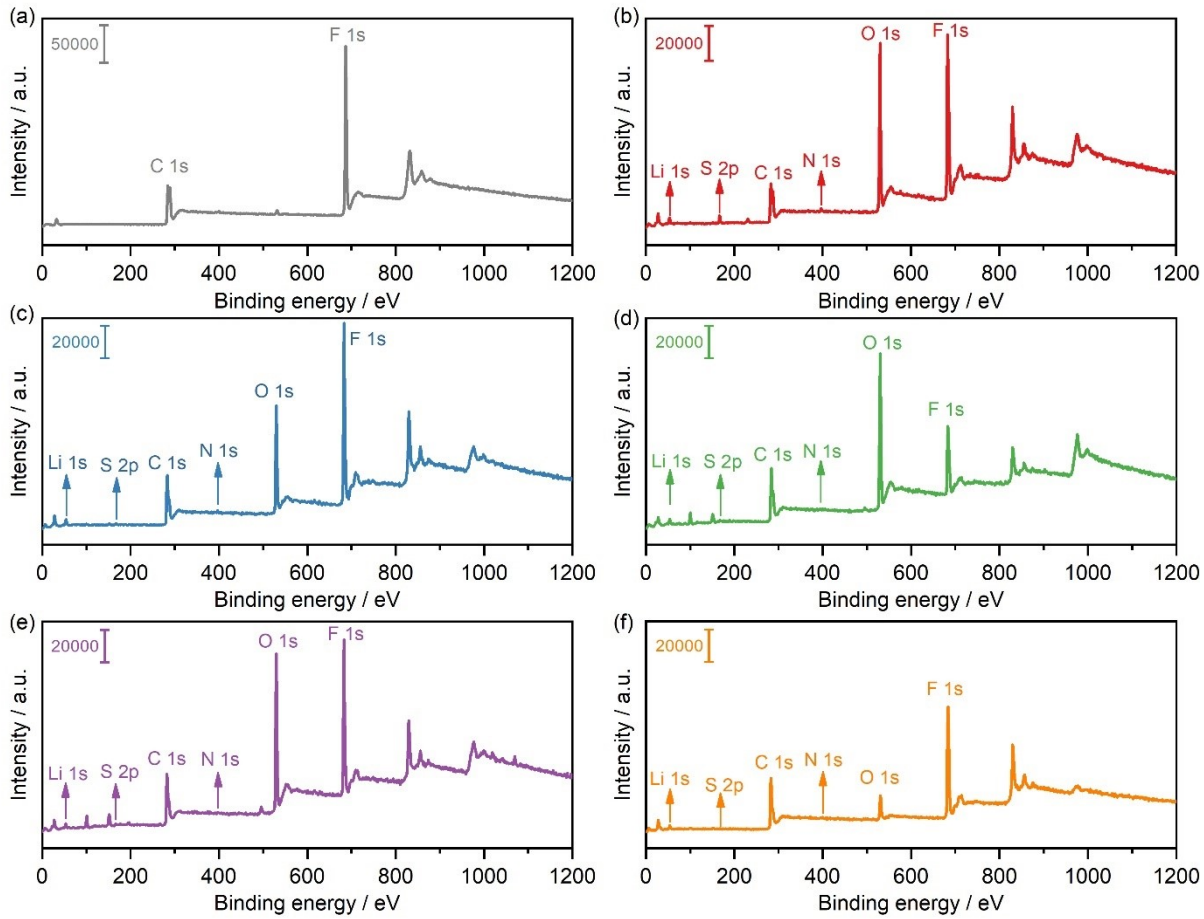

Fig. S13 XPS survey spectra for pristine fluorinated carbon (a) and the electrodes after discharge at 0.1C with various kinds of electrolytes (b-f). (b) $D_{100}P_0$, (c) $D_{70}P_{30}$, (d) $D_{50}P_{50}$, (e) $D_{30}P_{70}$, and (f) D_0P_{100}.

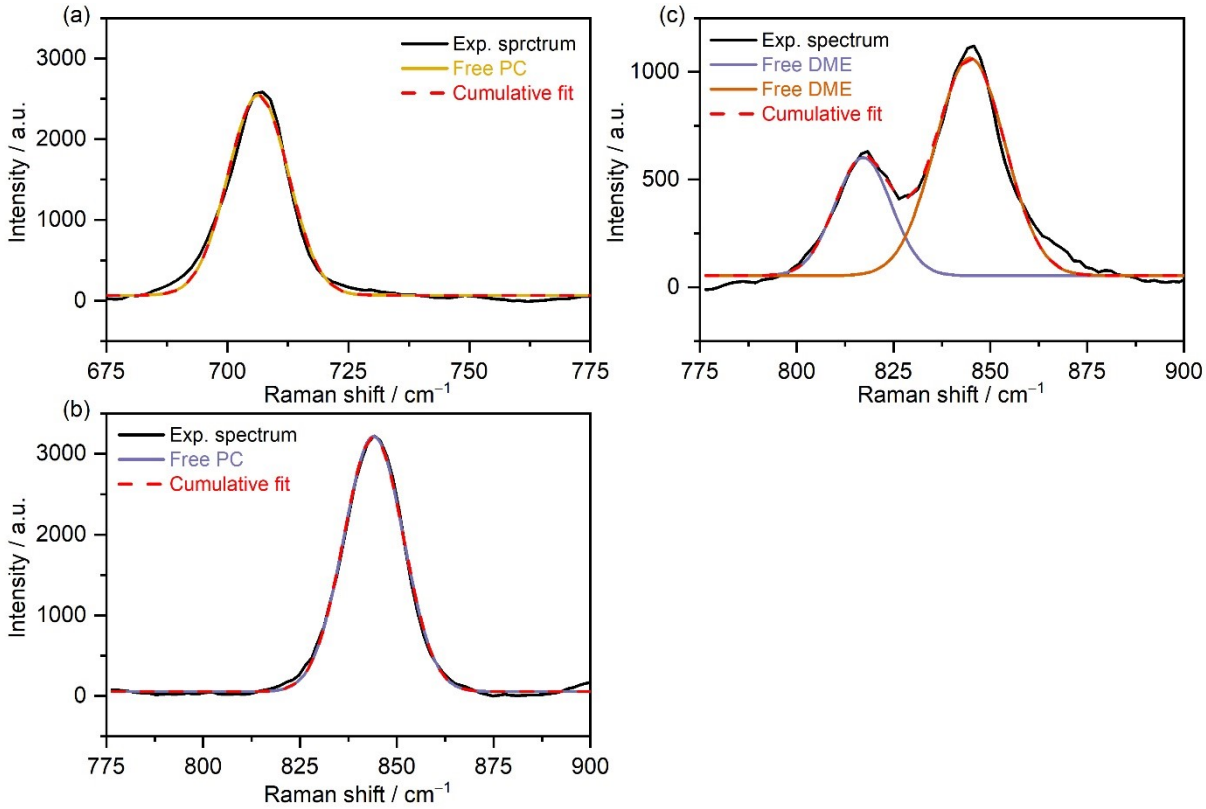

Fig. S14 Local Raman spectra and solution composition diagram of the neat PC and DME: (a) neat PC in the region 675–775 cm^{-1}; (b) neat PC in the region 775–900 cm^{-1}; (c) neat DME in the region 775–900 cm^{-1}.

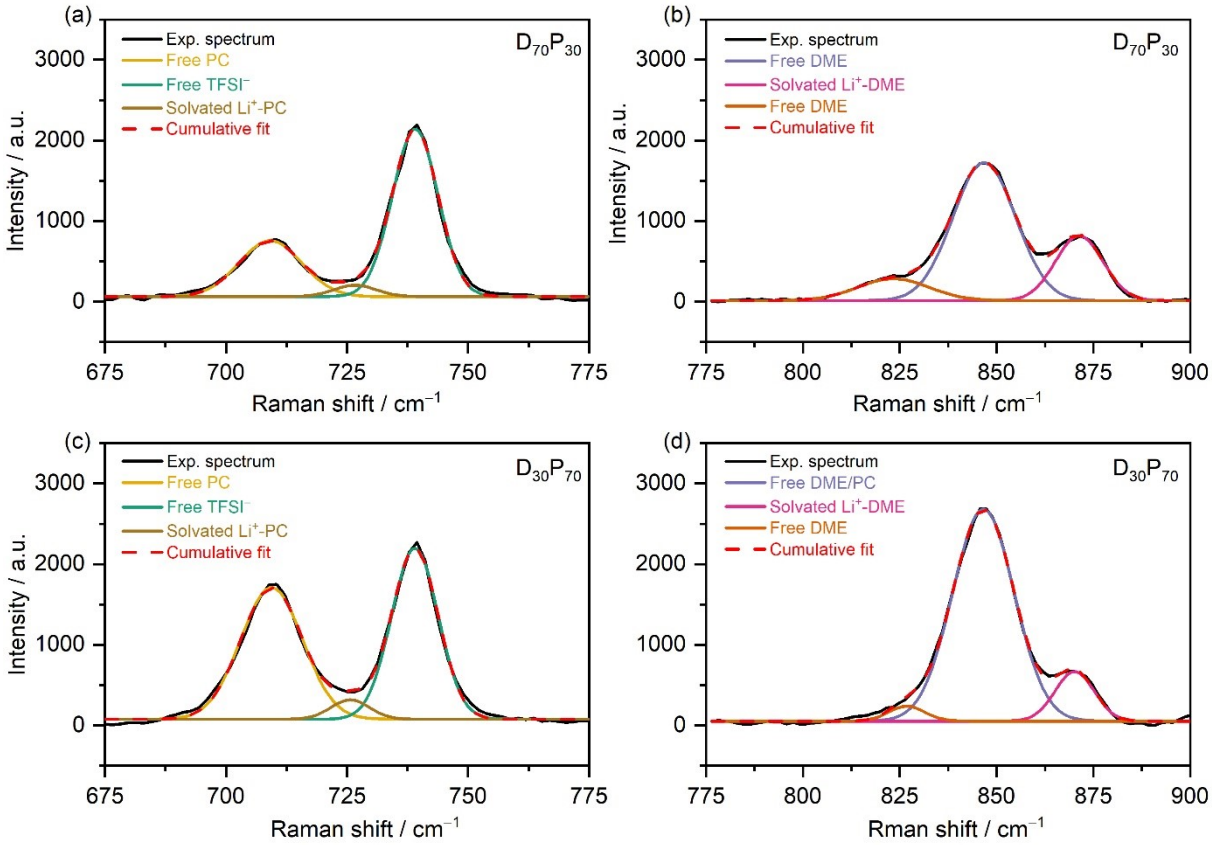

Fig. S15 Local Raman spectra and solution composition diagram of the selected electrolytes: (a) $D_{70}P_{30}$ electrolyte in the region 675–775 cm^{-1}; (b) $D_{70}P_{30}$ electrolyte in the region 775–900 cm^{-1}; (c) $D_{30}P_{70}$ electrolyte in the region 675–775 cm^{-1}; (d) $D_{30}P_{70}$ electrolyte in the region 775–900 cm^{-1}.

References

1. I. Smallwood, *Handbook of organic solvent properties*, Butterworth-Heinemann, **2012**.
2. H. Zhang, C. Li, M. Piszcz, E. Coya, T. Rojo, L. M. Rodriguez-Martinez, M. Armand and Z. Zhou, *Chem. Soc. Rev.*, 2017, **46**, 797–815.
3. H. Zhang, U. Oteo, H. Zhu, X. Judez, M. Martinez-Ibañez, I. Aldalur, E. Sanchez-Diez, C. Li, J. Carrasco, M. Forsyth and M. Armand, *Angew. Chem., Int. Ed.*, 2019, **58**, 7829–7834.
4. L. Qiao, U. Oteo, M. Martinez-Ibanez, A. Santiago, R. Cid, E. Sanchez-Diez, E. Lobato, L. Meabe, M. Armand and H. Zhang, *Nat. Mater.*, 2022, **21**, 455–462.
5. X. Wang, Z. Song, H. Wu, H. Yu, W. Feng, M. Armand, X. Huang, Z. Zhou and H. Zhang, *Angew. Chem., Int. Ed.*, 2022, **61**, e202211623.
6. H. Wu, Z. Song, W. Feng, Z. Zhou and H. Zhang, *Nano Res.*, 2023, **16**, 9507–9518.
7. D. S. Hall, J. Self and J. R. Dahn, *J. Phys. Chem. C*, 2015, **119**, 22322–22330.
8. M. Schmeisser, P. Illner, R. Puchta, A. Zahl and R. van Eldik, *Chemistry*, 2012, **18**, 10969–10982.
9. W. Weppner and R. A. Huggins, *J. Electrochem. Soc.*, 1977, **124**, 1569–1578.
10. L. Li, R. Jacobs, P. Gao, L. Gan, F. Wang, D. Morgan and S. Jin, *J. Am. Chem. Soc.*, 2016, **138**, 2838–2848.
11. Y. Xiao, J. Jian, A. Fu, C. Tang, Y. Zou, X. Chen, J. Wang, Y. Yang and J. Zheng, *ACS Sustainable Chem. Eng.*, 2022, **10**, 6217–6229.
12. V. Blum, R. Gehrke, F. Hanke, P. Havu, V. Havu, X. Ren, K. Reuter and M. Scheffler, *Comput. Phys. Commun.*, 2009, **180**, 2175–2196.
13. V. Havu, V. Blum, P. Havu and M. Scheffler, *J. Comput. Phys.*, 2009, **228**, 8367–8379.
14. C. Lee, W. Yang and R. G. Parr, *Phys. Rev. B*, 1988, **37**, 785–789.
15. A. D. Becke, *J. Chem. Phys.*, 1992, **96**, 2155–2160.
16. M. D. Hanwell, D. E. Curtis, D. C. Lonie, T. Vandermeersch, E. Zurek and G. R. Hutchison, *J. Cheminform.*, 2012, **4**, 1–17.
17. H. Zhang, O. Arcelus and J. Carrasco, *Electrochim. Acta*, 2018, **280**, 290–299.
18. M. Martinez-Ibañez, E. Sanchez-Diez, L. Qiao, Y. Zhang, X. Judez, A. Santiago, I. Aldalur, J. Carrasco, H. Zhu, M. Forsyth, M. Armand and H. Zhang, *Adv. Funct. Mater.*, 2020, **30**, 2000455.
19. X. Wang, Z. Song, H. Wu, J. Nie, W. Feng, H. Yu, X. Huang, M. Armand, Z. Zhou and H. Zhang, *ChemElectroChem*, 2022, **9**, e202101590.
20. E. Grunwald and S. Winstein, *J. Am. Chem. Soc.*, 1948, **70**, 846–854.
21. S. Winstein, E. Grunwald and H. W. Jones, *J. Am. Chem. Soc.*, 1951, **73**, 2700–2707.
22. A. H. Fainberg and S. Winstein, *J. Am. Chem. Soc.*, 1957, **79**, 1597–1602.
23. J. A. Berson, Z. Hamlet and W. A. Mueller, *J. Am. Chem. Soc.*, 1962, **84**, 297–304.
24. E. M. Kosower, *J. Am. Chem. Soc.*, 1958, **80**, 3253–3260.
25. K. Dimroth, C. Reichardt, T. Siepmann and F. Bohlmann, *Justus Liebigs Ann. Chem.*, 1963, **661**, 1–37.
26. C. Reichardt, *Angew. Chem., Int. Ed.*, 1965, **4**, 29–40.
27. P. Huang, X. Liu, Y. Wada, K. Katoh, M. Arai and M. Tamura, *Fuel*, 2013, **105**, 364–367.
28. P. N. Le Pham, V. Gabaudan, A. Boulaoued, G. Åvall, F. Salles, P. Johansson, L. Monconduit and L. Stievano, *Energy Storage Mater.*, 2022, **45**, 291–300.
29. D. Battisti, G. A. Nazri, B. Klassen and R. Aroca, *J. Phys. Chem.*, 1993, **97**, 5826–5830.
30. Z. Wang, W. Gao, X. Huang, Y. Mo and L. Chen, *J. Raman Spectrosc.*, 2001, **32**, 900–905.
31. J. L. Allen, O. Borodin, D. M. Seo and W. A. Henderson, *J. Power Sources*, 2014, **267**, 821–830.
32. Y.-S. Kim and S.-K. Jeong, *J. Spectrosc.*, 2015, **2015**, 323649.
33. L. Suo, F. Zheng, Y.-S. Hu and L. Chen, *Chin. Phys. B*, 2016, **25**, 016101.
34. N. Xiao, W. D. McCulloch and Y. Wu, *J. Am. Chem. Soc.*, 2017, **139**, 9475–9478.
35. P. Zeng, Y. Han, X. Duan, G. Jia, L. Huang and Y. Chen, *Mater. Res. Bull.*, 2017, **95**, 61–70.
36. J. Ming, Z. Cao, Y. Wu, W. Wahyudi, W. Wang, X. Guo, L. Cavallo, J.-Y. Hwang, A. Shamim, L.-J. Li, Y.-K. Sun and H. N. Alshareef, *ACS Energy Lett.*, 2019, **4**, 2613–2622.
37. R. Konefał, Z. Morávková, B. Paruzel, V. Patsula, S. Abbrent, K. Szutkowski and S. Jurga, *Polymers*, 2020, **12**, 1595.
38. M. Martinez-Ibañez, N. Boaretto, L. Meabe, X. Wang, H. Zhu, A. Santiago, O. Zugazua, M. Forsyth, M. Armand and H. Zhang, *Chem. Mater.*, 2022, **34**, 7493–7502.
39. A. Eshaghi and M. Salehi, *Opt. Quantum Electron.*, 2018, **50**, 431.
40. S. Li, J.-H. Lee, S. M. Hwang, J.-B. Yoo, H. Kim and Y.-J. Kim, *Energy Storage Mater.*, 2021, **41**, 466–474.
41. C.-M. Park, J.-H. Kim, H. Kim and H.-J. Sohn, *Chem. Soc. Rev.*, 2010, **39**, 3115–3141.
42. Q. Su, D. Xie, J. Zhang, G. Du and B. Xu, *ACS Nano*, 2013, **7**, 9115–9121.
43. Y.-D. Ko, J.-G. Kang, K. J. Choi, J.-G. Park, J.-P. Ahn, K. Y. Chung, K.-W. Nam, W.-S. Yoon and D.-W. Kim, *J. Mater. Chem.*, 2009, **19**, 1829–1835.
44. M. Akbari Garakani, S. Abouali, J. Cui and J.-K. Kim, *Mater. Chem. Front.*, 2018, **2**, 1481–1488.
45. S. Liu, J. Xie, Q. Su, G. Du, S. Zhang, G. Cao, T. Zhu and X. Zhao, *Nano Energy*, 2014, **8**, 84–94.
46. J. Y. Cheong, J. H. Chang, C. Kim, J. Lee, Y.-S. Shim, S. J. Yoo, J. M. Yuk and I.-D. Kim, *ACS Appl. Energy Mater.*, 2019, **2**, 2004–2012.
47. J. F. S. Fernando, C. Zhang, Konstantin L. Firestein, J. Y. Nerkar and D. V. Golberg, *J. Mater. Chem. A*, 2019, **7**, 8460–8471.

48. P. G. Bruce, S. A. Freunberger, L. J. Hardwick and J. M. Tarascon, *Nat. Mater.*, 2011, **11**, 19–29.
49. Q. Su, J. Xie, J. Zhang, Y. Zhong, G. Du and B. Xu, *ACS Appl. Mater. Interfaces*, 2014, **6**, 3016–3022.
50. J. Zou, J. Zhao, B. Wang, S. Chen, P. Chen, Q. Ran, L. Li, X. Wang, J. Yao, H. Li, J. Huang, X. Niu and L. Wang, *ACS Appl. Mater. Interfaces*, 2020, **12**, 44850–44857.
51. M. G. Boebinger, M. Xu, X. Ma, H. Chen, R. R. Unocic and M. T. McDowell, *J. Mater. Chem. A*, 2017, **5**, 11701–11709.
52. B. Han, S. Chen, J. Zou, R. Shao, Z. Dou, C. Yang, X. Ma, J. Lu, K. Liu, D. Yu, L. Wang, H. Wang and P. Gao, *Nanoscale*, 2019, **11**, 7474–7480.
53. S. Hwang, Z. Yao, L. Zhang, M. Fu, K. He, L. Mai, C. Wolverton and D. Su, *ACS Nano*, 2018, **12**, 3638–3645.
54. Z. Ma, Z. Yao, Y. Cheng, X. Zhang, B. Guo, Y. Lyu, P. Wang, Q. Li, H. Wang, A. Nie and A. Aspuru-Guzik, *Nano Energy*, 2020, **67**, 104276.
55. Q. Li, P. Du, Y. Yuan, W. Yao, Z. Ma, B. Guo, Y. Lyu, P. Wang, H. Wang, A. Nie, R. Shahbazian-Yassar and J. Lu, *Nano Lett.*, 2019, **19**, 3074–3082.
56. L. Li, F. Meng and S. Jin, *Nano Lett.*, 2012, **12**, 6030–6037.
57. C. Villa, S. Kim, Y. Lu, V. P. Dravid and J. Wu, *ACS Appl. Mater. Interfaces*, 2019, **11**, 647–654.
58. F. Wang, S. W. Kim, D. H. Seo, K. Kang, L. Wang, D. Su, J. J. Vajo, J. Wang and J. Graetz, *Nat. Commun.*, 2015, **6**, 6668.
59. S. Shi, Z. Li, Y. Sun, B. Wang, Q. Liu, Y. Hou, S. Huang, J. Huang and Y. Zhao, *Nano Energy*, 2018, **48**, 510–517.
60. J. Liang, G. Zhu, Y. Zhang, H. Liang and W. Huang, *Nano Res.*, 2021, **15**, 2023–2029.
61. Y. Ding, T. Han, H. Zhang, M. Cheng, Y. Wu, X. Chen, M. Chi, J. Niu and J. Liu, Appl. Surf. Sci., 2019, 490, 510–515.
62. Wohlfarth, C. *Permittivity (Dielectric Constants) of Liquids. In CRC Handbook of Chemistry and Physics* (Internet Version 2015); Haynes, W. M., Ed.; CRC Press/Taylor and Francis: Boca Raton, FL, 2015.
63. Y. Matsuda, H. Nakashima, M. Morita and Y. Takasu, *J. Electrochem. Soc.*, 1981, **128**, 2552–2556.
64. M. Ue and S. Mori, *J. Electrochem. Soc.*, 1995, **142**, 2577–2581.